Simulating Future Exposure to Coastal Urban Flooding Using a Neural Network–Markov Model

Ayyoub Frifra, Mohamed Maanan, Mehdi Maanan, Hassan Rhinane

Journal of
Marine Science and Engineering

MDPI

Article

Simulating Future Exposure to Coastal Urban Flooding Using a Neural Network–Markov Model

Ayyoub Frifra [1,2,3], Mohamed Maanan [1,*], Mehdi Maanan [2] and Hassan Rhinane [2]

[1] UMR 6554 CNRS LETG-Nantes Laboratory, Institute of Geography and Planning, Nantes University, 44312 Nantes, France; ayyoub.frifra@univ-nantes.fr
[2] Geosciences Laboratory, Faculty of Sciences Ain Chock, Hassan II University of Casablanca, Casablanca 20100, Morocco; mehdi.maanan@gmail.com (M.M.); h.rhinane@gmail.com (H.R.)
[3] Department of Geomorphology and Geomatics, Scientific Institute, Mohammed V University in Rabat, Rabat 10106, Morocco
* Correspondence: mohamed.maanan@univ-nantes.fr

Abstract: Urbanization and climate change are two major challenges of the 21st century, and the effects of climate change, combined with the urbanization of coastal areas, increase the frequency of coastal flooding and the area exposed to it, resulting in increased risk of flooding and larger numbers of people and properties being vulnerable. An urban growth modeling system was used to simulate future growth scenarios along the coast of the Vendée region in western France, and the potential exposure to flooding with each scenario was evaluated. The model used was an Artificial Neural Network combined with a Markov Chain, using data obtained by the remote sensing and geographic information system techniques to predict three future urban growth scenarios: business as usual, environmental protection, and strategic urban planning. High-risk flood areas and future sea level projections from the Sixth Assessment Report of the Intergovernmental Panel on Climate Change were then used to assess future flood risk under each growth scenario in the study area. According to the results, the different growth scenarios are associated with different development patterns, and the strategic urban planning scenario significantly reduces the risk of flooding compared to the other two scenarios. However, the rise in sea level considerably expands the areas vulnerable to flooding. Finally, the methodology adopted can be used to prepare for the impact of climate change and develop strategies to mitigate the risk of flooding in the future.

Keywords: urban growth modeling; climate change; sea level rise; flood risk; urban flood exposure; artificial neural network–Markov chain model

Citation: Frifra, A.; Maanan, M.; Maanan, M.; Rhinane, H. Simulating Future Exposure to Coastal Urban Flooding Using a Neural Network–Markov Model. *J. Mar. Sci. Eng.* **2024**, *12*, 800. https://doi.org/10.3390/jmse12050800

Academic Editor: João Miguel Dias

Received: 14 April 2024
Revised: 8 May 2024
Accepted: 8 May 2024
Published: 11 May 2024

1. Introduction

Urbanization and climate change are major issues in the 21st century [1,2]. Urban areas in general are developing quickly and are projected to increase by 1.2 million km^2 by 2030 [3]. Urbanization is more concentrated and intricate in coastal areas [4] and it is expanding at a substantially faster rate than in non-coastal locations. In China, for example, urban areas on the coast are expanding three times faster than the national average [5]. Coastal locations are appealing to people because of several economic and geographic considerations [5]. Most of the world's megacities are situated on the coast [6], where the largest concentrations of people and property may be found [7]. However, urbanization leads to higher susceptibility to coastal flooding due to the increased likelihood of tropical and extratropical storms causing significant damage when they make landfall [7]. Coastal floods caused by severe storm surges are highly dangerous and economically destructive to coastal regions [8,9]. An estimated 200 million people worldwide are currently at risk of coastal flooding [10], and their number is expected to increase in the 21st century [11].

In France, the western coast has been subject to several floods caused by storms, such as the extensive flood that occurred as a result of Storm Xynthia in February 2010,

causing 47 deaths and at least 2.5 billion euros' worth of damage [9]. 46 coastal floods have been observed in the area during the previous 500 years, showing the high degree of vulnerability of the region [9]. Climate change is anticipated to increase the frequency of storms in the mid-latitudes [12], marked with more storm surges and higher waves, which will increase the risk and vulnerability of the west coast of France. The Intergovernmental Panel on Climate Change (IPCC) has also predicted that the mean sea level would continue to rise over the course of the 21st century as a result of climate change [13]. Consequently, if future urban growth is not appropriately planned, the combination of sea level rise, higher storm wave height, and more storm surges would exacerbate the situation, leading to increased susceptibility to coastal flooding.

Urban growth modeling may be used to develop sustainable urban planning by simulating various urban expansion scenarios, evaluating the potential exposure to flooding associated with different scenarios, and identifying the best direction for future growth. A literature review revealed that various models have been used in the past to simulate future urban growth, for example Cellular Automata (CA) [14,15], Artificial Neural Networks (ANN) [16], random forest-cellular automata [17], SLEUTH [18,19], ANN-CA [20,21], CA-Markov [22,23], Markov and genetic algorithm [24], and ANN-Markov [25].

A model combining a multi-layer perceptron (MLP) with a Markov chain (MLP–Markov) was utilized for this study because of its efficiency in forecasting future urban expansion in many prior studies [25–27]. The MLP is a kind of ANN commonly utilized in urban development modeling [25,26], comprising an input layer, one or more hidden layers, and an output layer. The MLP is based on the backpropagation algorithm and integrates the selected driving variables of urban growth to predict transition potentials between two time periods in a given location [25]. The combined MLP–Markov model is used extensively for modeling complex behaviors and patterns; it can handle numerous input variables and operate without prior knowledge, unlike other modeling methods, such as Sleuth, which requires coefficient values to be set, and cellular automata methods, which require a suitability map based on prior knowledge of change behavior [26].

According to the literature, most urban growth modeling studies focus on estimating the potential impacts of urban expansion and determining the best direction for future urban growth [8,28–34]. While the effects of climate change on future urban expansion have received little attention, only a few studies have looked at how climate change, especially sea level rise, affects future urban development. For example, Huong and Pathirana investigated urban floods caused by climate-driven sea level rise in Can Tho, Vietnam, using a land use simulation model that estimates urban development up to the year 2100 based on historical growth trends [35]. Lu et al. employed a fuzzy cellular automata-based Markov chain model to anticipate future land use changes in New York City for the years 2030 and 2050, taking into account projected sea level rise and long-term rainfall-runoff flooding consequences caused by climate change [36]. Similarly, Song et al. used the cellular-automaton-based SLEUTH model to anticipate future urban exposure to shifting sea levels in Bay County, Florida [37]. These studies are confined to projecting a single growth scenario based on historical growth patterns, or scenarios that simply present alternate development patterns. Very few studies, to the best of our knowledge, have linked urbanization based on diverse growth scenarios with climate change and flood risk [4]. This study fills this gap in the research and contributes further to the field of urban growth modeling by simulating future urban development along the coastal areas of the Vendée region, with three different urban growth scenarios (business as usual, environmental protection, and strategic urban planning), providing a comprehensive picture of how various growth paths interact with climate change and flood hazards, and applying the MLP–Markov model, which is rarely applied for estimating future urban flood exposure. This study does not consider the shoreline retreat, which will be addressed in a separate future study to assess the susceptibility of the study region to erosion.

This study examines the use of an urban development modeling technique, specifically a combined MLP–Markov model, to simulate three future urban expansion scenarios

in the Vendée coastal region of western France. These urban expansion scenarios are evaluated to determine their potential susceptibility to flooding, taking into account high-risk flood zones as well as future sea level estimates. The primary goal of the research is to aid in sustainable urban planning and flood risk reduction by detecting and evaluating the potential effects of severe storm events and rising sea levels on future urban flood vulnerability. The importance of this study stems from its comprehensive methodology, which includes the use of the seldom utilized MLP–Markov model to anticipate how diverse development strategies would influence future urban flood risk in response to extreme storms and increasing sea levels. To offer a complete explanation of the methodology underlying this research, the study is divided into numerous parts: The 'Materials and Methods' section starts by stating the subject region. It then describes the data and technique employed. Following that, the 'Results and Discussion' section presents the study's results, evaluates their significance and limitations, and proposes further research. Finally, the 'Conclusions' section provides a summary of the study's key results.

2. Materials and Methods

2.1. Study Area

The study area is situated in the Vendée region on the mid-Atlantic coast of France, between the Bay of Bourgneuf and the Bay of L'Aiguillon (Figure 1). The Vendée coast spans around 276 km in a NWS–E direction and is comprised of three main types: 64 km of rocky coastline, 109 km of sandy beaches, and 103 km of sea defenses [38]. The study analysis also covers small areas of the coast in the adjacent Charente-Maritime region, including Ré island.

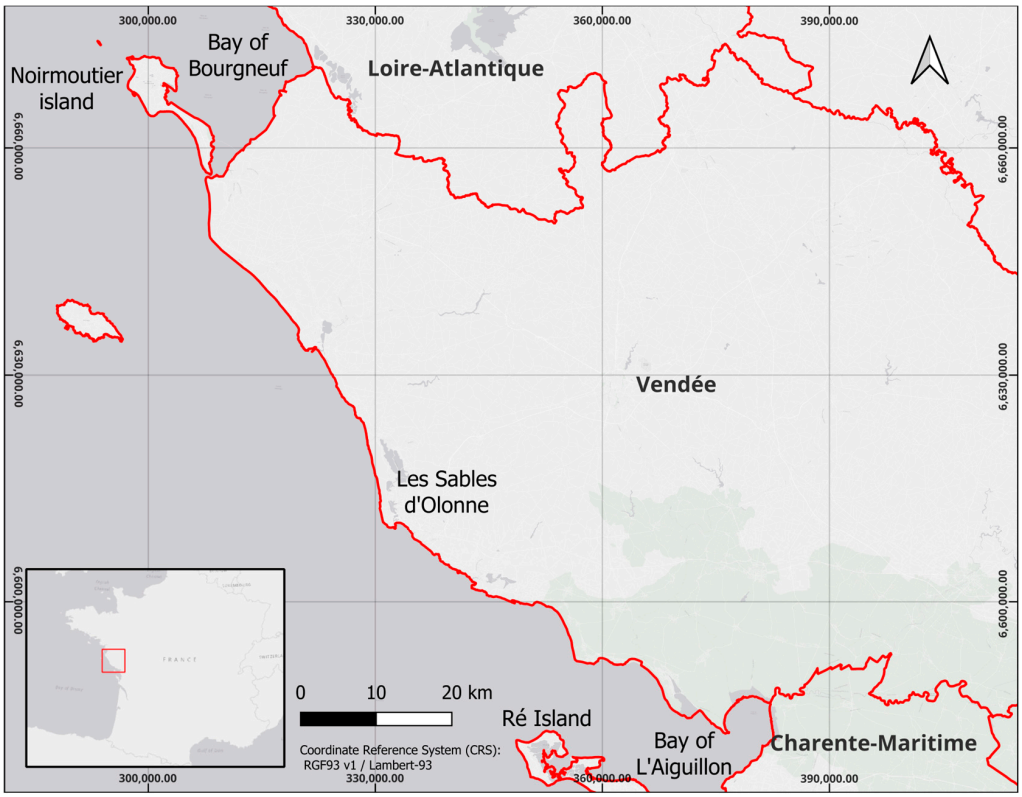

Figure 1. Location of the study area.

The research area has seen significant coastal flooding due to severe winter storms, resulting in substantial property damage and loss of life [39–41]. The rising probability of storms [42] and ongoing sea level rise forecasted for the 21st century [13], together with urban growth, will lead to more frequent floods and impact wider regions in the study area.

2.2. Data Used

Surface reflectance data from Landsat 5 and 8 were used to create land use land cover (LULC) maps for the research region in 2006, 2019, and 2022. The images were filtered according to the research area, and clouds and cloud shadows were removed using the CFMask technique, which is a C code based on the Function of Mask (Fmask). This approach surpasses existing cloud and cloud shadow masking techniques in terms of overall accuracy [43]. The median temporal aggregation method was then applied to decrease the data amount while maintaining a high degree of accuracy, as demonstrated by Noi Phan et al. [44]. Median images were computed for the years 2006, 2019, and 2022 by using all scenes available for each year on the Google Earth Engine (GEE) platform. The resulting LULC maps were then used for examining historical urban development and predicting future urban expansion.

Table 1 illustrates the auxiliary data utilized in this investigation, including the 25-m digital elevation model (DEM) obtained from the BD ALTI® database, and used to construct a slope map of the study region. Road network data was taken from the ROUTE 500® database, and coastline boundary data from the LIMITE TERRE–MER database. Data from the Protected Areas program were utilized to define protected zones within the research area. The Natural Risk Prevention Plan (PPRN), available on the Géorisques website, was used to integrate the urban plan of the study area, as produced by the local planning authority, into the urban growth prediction for the study. The PPRN aims to reinforce environmental protection and prevent natural risks by applying enforceable regulations depending on the level of hazard. Urbanization is limited or prohibited where the hazard and stakes are high. The above data were used to derive the modeling variables needed to predict future urban growth in the study area.

Table 1. Data used in the study.

Data	Format	Data Source	Year	Resolution
DEM	Raster	BD ALTI® https://geoservices.ign.fr/bdalti, accessed on 23 February 2023	2022	25 m
Road network	Vector	ROUTE 500® https://geoservices.ign.fr/route500, accessed on 3 March 2023	2021	N/A
Coastal boundary	Vector	LIMITE TERRE-MER https://geoservices.ign.fr/limite-terre-mer, accessed on 3 March 2023	2021	N/A
Protected zones	Vector	INPN—Données du programme 'Espaces Protégés' https://www.data.gouv.fr/fr/datasets/inpn-donnees-du-programme-espaces-proteges/#/resources, accessed on 10 March 2023	2022	N/A
Natural Risk Prevention Plan	Vector	Plans de Préventions des Risques naturels https://www.georisques.gouv.fr/plans-de-prevention-des-risques-naturels, accessed on 10 March 2023	2023	N/A
High-risk flood areas	Vector	Territoires à Risques important d'Inondation (TRI)—version 2 https://www.georisques.gouv.fr/donnees/bases-de-donnees/zonages-inondation-rapportage-2020, accessed on 10 March 2023	2020	N/A
Future sea level projection	CSV formatted	This data produced by the IPCC authors and supplied for archiving at the Centre for Environmental Data Analysis (CEDA) https://catalogue.ceda.ac.uk/uuid/98af2184e13e4b91893ab72f301790db, accessed on 10 March 2023	2060/ 2100	N/A

High-risk flood areas are areas that are highly vulnerable to flooding in the event of an extreme storm; this was used in conjunction with IPCC future sea level projection data (the SSP5-8.5 Low Confidence scenario) to assess the risk of floods in the study area in the future [13].

2.3. Method

To achieve the above study objectives, the research roadmap involved three main steps: (a) LULC classification; (b) urban growth modeling; and (c) assessment of potential exposure to urban flooding (Figure 2).

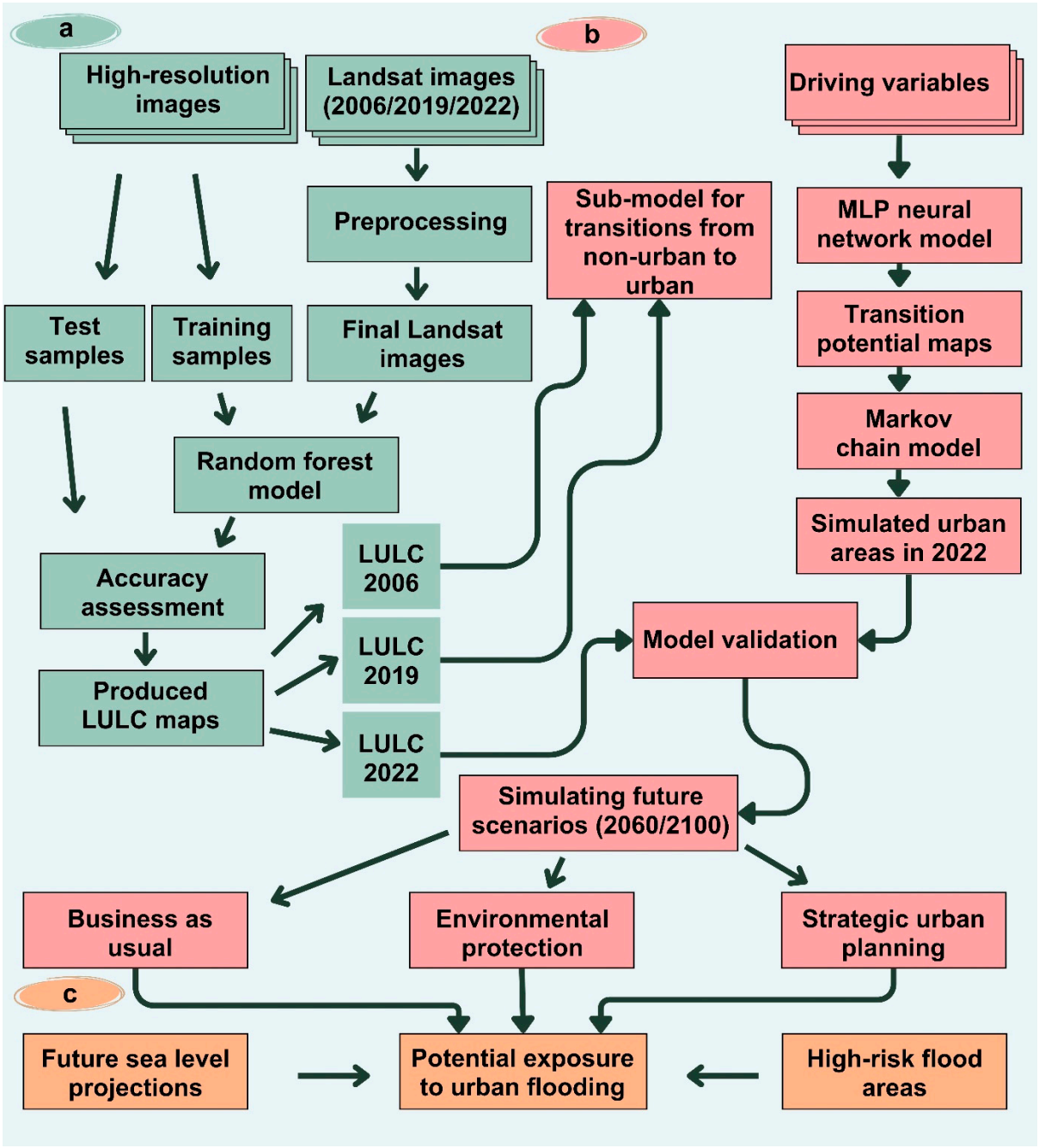

Figure 2. Research methodology: (**a**) LULC classification; (**b**) Urban growth modeling; (**c**) Assessment of potential exposure to urban flooding.

Prior to LULC classification, the Landsat images were subjected to preprocessing techniques, including filtering, cloud and cloud shadow masking, and median temporal aggregation. Subsequently, a random forest classifier was utilized in GEE for the classification operation. The training and validation samples were obtained by visually interpreting high-resolution images. The model's performance was measured using the Overall Accuracy (OA) and Kappa coefficient (K) measures.

Next, the step of modeling urban growth includes the usage of the Land Change Modeler (LCM) within the TerrSet 2020 v.19.0.7 Geospatial Monitoring and Modeling software to produce a combined MLP–Markov model. The combined model was used to anticipate future urban growth in the study region using six driving factors, which were selected based on prior research and area characteristics. Initially, the study centered on changes between 2006 and 2019 to construct a sub-model, particularly for transitions from non-urban regions to urban areas. Afterwards, an MLP neural network was utilized to merge the sub-model and selected driving variables to forecast transition potentials. Subsequent potential transition maps were created to depict the possibility of change from non-urban to urban locations within the research area. The Markov chain model was then used to compute transition probabilities for future predictions, relying on observable changes from 2006 to 2019, and to simulate LULC maps for 2022. The study examined three separate scenarios for forecasting future urban growth: business as usual, environmental protection, and strategic urban planning. Each scenario was specified by numerous development restrictions and limits, which influenced the expected urban growth patterns.

Third, the validation of the model entails comparing the simulated LULC maps with the actual 2022 LULC map, employing multiple evaluation metrics.

Finally, after the confirmation of the model prediction, future urban expansion scenarios were simulated for the years 2060 and 2100. The assessment of possible exposure of future urban expansion to flood risks in each growth scenario was then performed by overlaying urban development scenarios with high-risk flood areas and anticipated sea level rise for 2060 and 2100.

2.3.1. LULC Classification

Five LULC classes were considered: water, forest, other land, agriculture, and urban. The "other land" class included all LULC classes not covered by the other four classes. The classification was performed using a random forest model, which has been widely used for classifying land cover with remote sensing data [45–48]. This model has been shown to outperform other machine learning classifiers, like support vector machine [49]. Random forest needs less processing time, fewer parameters and less manual intervention [50,51]. It is the most frequently used method for classifying satellite images in GEE, according to an analysis of 349 peer-reviewed studies published within the last decade [52]. Random forest is an ensemble learning technique that uses several decision trees to enhance the accuracy of classification [53]. This method generates multiple binary classification and regression trees by creating subsets of the input data using a process called bootstrapping. Bootstrapping includes randomly selecting the data with replacement [54]. Every tree in the forest divides the data by employing a subset of variables that are randomly chosen at each node. This process increases the diversity among the trees and decreases the variability of the model. Random forest trees, unlike traditional decision trees, are not pruned, enabling them to build sophisticated structures that accurately reflect complex patterns in the data. During the process of classification, an unseen sample is individually classified by each tree in the forest. The final output class is then selected by a majority vote among all the trees. Aggregating many decision trees helps to reduce the problem of overfitting, which is often seen in individual decision trees. This results in more trustworthy and consistent predictions over a wide range of circumstances. A random forest classifier with 300 trees and 5 randomly-selected variables per split was therefore run in GEE to create LULC maps of the study region. High-resolution images, including orthophoto images with a spatial resolution of 0.2 m for the years 2022 and 2019, obtained from the BD ORTHO® database, and an aerial image for the year 2006 with a resolution of 0.7 m from the National Institute of Geographic and Forestry Information (IGN) website, were manually visually interpreted to gather training and validation samples. 6370 points were chosen randomly from the LULC classes and divided into training and validation sets at a ratio of 80 to 20. The OA and K performance measures were used to assess the classification accuracy; these metrics,

taken from the confusion matrices, have been used in many similar studies to evaluate the accuracy of LULC classification. Further information can be found in the literature [48].

2.3.2. Urban Growth Modeling

After creating the LULC maps, the third part of the research consists of modeling future urban expansion within the study region. This is accomplished through the utilization of a combined MLP–Markov model, developed using the LCM in the TerrSet 2020 v.19.0.7 software. The LCM is a modeling system widely used for LULC change analysis, prediction, and scenario simulation [27,30], and is an efficient tool for urban planning and sustainable development [4]. The simulation of urban expansion using the MLP–Markov model involved four sub-steps: selection of driving variables, transition potential modeling, scenario setting for future urban growth simulation, and model validation.

Selection of Driving Variables

In urban growth modeling, it is crucial to select the appropriate driving variables, as these affect the accuracy of the LULC transitions that are simulated from the transitions observed [25]. Numerous studies have found that the drivers of urban expansion vary depending on the characteristics of the study area, and their effects on LULC change vary across different locations and over time, especially where extreme events are common [25,26,55–57]. Based on past research and study area characteristics, we therefore selected six variables as the drivers of urban growth: DEM, slope, distance to major roads, distance to coast, distance to existing urban area, and evidence likelihood.

DEM and slope were selected as driving factors because of their major impact on urban expansion, indicating potential regions for future development. For example, lowland regions are more likely to be developed. Similarly, since major roads are the primary mode of transit propelling urbanization, their proximity has a significant impact on future growth. Coastal proximity seems a crucial feature shaping future development. Areas along the coast are more appealing for development owing to the scenic views, recreational activities, and proximity to maritime industries. Furthermore, distance to existing urban areas impacts urban expansion, with new built-up regions often sprouting around established urban centers. Moreover, the evidence likelihood is significant because it converts categorical variables, such as changes between different land cover classes, into numerical values that can be applied in the modeling procedure.

Previous studies have identified these variables as key drivers of urban development [4,27]. The DEM was used to extract the slope, and the Euclidean distance method was used to generate other distance-based variables. The evidence likelihood was computed using the LCM evidence likelihood tool. Finally, all the drivers were rasterized at a spatial resolution of 30 m.

Transition Potential Modeling

The second sub-step of urban growth simulation entails transition-potential modeling. First, the analysis focused on transitions occurring between 2006 and 2019 to generate a sub-model for non-urban to urban transitions. According to Abuelaish and Olmedo [58], a sub-model refers to a collection of transitions that can be modeled collectively and are impacted by the same forces. All transitions from the various non-urban LULC types to urban-type were combined into a single sub-model to compute transition potentials. An MLP neural network, integrating the generated sub-model and the selected driving variables, was then used to create potential transition maps illustrating the potential of each transition at any given location in the overall study area. For this study, the MLP neural network was run at 10,000 iterations using dynamic automatic training with a learning rate ranging from 0.0025 to 0.00025, a momentum factor at 0.5, a sigmoid constant of 1, and an acceptable error of 0.01. An accuracy value of 81.11% was achieved with the MLP neural network, corresponding to the measure of model calibration and within the recommended range of around 80% described in previous literature [4,27,30]. After calibrating the MLP model and creating the potential transition maps, the Markov chain model was

used to compute the transition probabilities expected in future predictions based on the 2006 to 2019 LULC changes. The Markov Chain model calculates transitions over time, whereas the MLP neural network predicts the transition potential of LULC changes between two time points in a given location [27].

Scenario Setting for Future Urban Growth Simulation

After the transition potential modeling sub-step, the LULC maps for 2022 were simulated to validate the model against the actual 2022 LULC map, using the transition matrix between 2006 and 2019. Three different scenarios—business as usual, environmental protection, and strategic urban planning—were investigated using the future urban expansion model (Table 2). The prediction of future urban growth under the business-as-usual scenario was based on historical urban expansion trends with no development regulations or restrictions. The existing urban areas and bodies of water, where no further growth could take place, were the only restricted areas in this initial scenario. The environmental-protection scenario, on the other hand, prioritized the protection and conservation of nature by limiting any further development in protected natural areas. The protected natural zones and restricted areas utilized in the business-as-usual scenario were incorporated in the constraints layer used in the MLP–Markov model in this scenario. Finally, the strategic-urban-planning scenario was based on the local urban plan of the research region, integrating development regulations from the Natural Risk Prevention Plan. The same restrictions as for the environmental-protection scenario were applied, together with restricted urbanization zones.

Table 2. Modeling Variables used for each urban growth scenario.

Modeling Variables	Urban Growth Scenarios		
	Business as Usual	**Environmental Protection**	**Strategic Urban Planning**
Drivers of urban growth	Digital elevation model Slope Distance to major roads Distance to coast Distance to existing urban area Evidence likelihood	Digital elevation model Slope Distance to major roads Distance to coast Distance to existing urban area Evidence likelihood	Digital elevation model Slope Distance to major roads Distance to coast Distance to existing urban area Evidence likelihood
Constraints	Existing urban areas Water bodies	Existing urban areas Water bodies Protected natural areas	Existing urban areas Water bodies Protected natural areas Restricted urbanization zones

Model Validation

After simulating the three scenarios for the 2022 LULC maps based on changes observed between 2006 and 2019, the MLP–Markov model was validated through the comparison of the predicted maps with the 2022 LULC map created in the LULC classification section (reference map). Various evaluation metrics were utilized, including Kappa for no ability (Kno), Kappa Kstandard, and Klocation (Table 3).

Table 3. Assessment metrics used for evaluating the MLP–Markov model.

Accuracy Measure	Definition	Range	Expected Minimum Threshold
Kno	Kno measures the overall accuracy of the simulated map by comparing the proportion of correctly predicted pixels with the anticipated proportion [59–61].	−1 to 1	>0.8
Kappa Kstandard	Kstandard assesses the map's ability to achieve perfect classification [59–61].	−1 to 1	>0.8
Klocation	Klocation assesses the simulation's accuracy based solely on location [59–61].	−1 to 1	>0.8
Quantity disagreement	Quantity disagreement represents the degree to which the predicted map fails to reflect the precise quantity of each LULC class, when compared to the reference map, not taking into account location [62].	0 to 100%	Overall disagreement (Quantity disagreement + Allocation disagreement) < 20%
Allocation disagreement	Allocation disagreement represents the degree to which the predicted map fails to reflect the precise position of each LULC class [62].	0 to 100%	Overall disagreement (Quantity disagreement + Allocation disagreement) < 20%
Overall agreement	Overall agreement is determined by omitting both quantity and allocation disagreement [62].	0 to 100%	>80%
Area under the curve (AUC)	Area under the curve is a quantitative measure derived from the Relative Operating Characteristic curve that compares the probability of a class occurring to its actual location [63,64].	0 to 1	>0.5

However, in a previous study, Pontius and Millones demonstrated that Kappa metrics can sometimes be ineffective or misleading, and recommended using quantity and allocation disagreements for accuracy evaluation and map comparison [62]. Quantity and allocation disagreements were therefore included to test the effectiveness of the model (Table 3).

In addition, the accuracy of the simulation was assessed using the area under the curve metric (AUC) taken from the Relative Operating Characteristic curve (ROC). The ROC approach is commonly used in land change science to validate simulations. It compares a suitability map depicting the likelihood of a class occurring with a map showing the actual location of the class [63,64].

2.3.3. Assessment of Potential Exposure to Urban Flooding

The potential vulnerability of the study region to flood risk in the future was examined using high-risk flood zones and future sea level projection data. Designation as a high-risk flood zone is based on three types of storm events, classified as scenarios: frequent event, average event, and exceptional event. According to the IPCC, the global mean sea level will continue to rise throughout the 21st century, according to five scenarios: SSP1-1.9, SSP1-2.6, SSP2-4.5, SSP3-7.0, and SSP5-8.5. The predicted global mean sea level rise by 2100 in the SSP5-8.5 medium-confidence scenario is 0.63–1.01 m, corresponding to very high greenhouse gas (GHG) emissions [65]. However, sea level estimates are fraught with uncertainty due to ice-sheet responses to warming. In this study, the SSP5-

8.5 low confidence scenario was selected, as it represents a low-likelihood, high-impact scenario with very high GHG emissions. This selected scenario is consistent with the low-risk tolerance in coastal safety planning in cities and takes into consideration the significant degree of uncertainty in ice-sheet responses to warming. In this scenario, ice-sheet processes could raise the global mean sea level to above the expected range before 2100 [65]. Given the extreme nature of this scenario and the need to prepare for worst-case scenarios to ensure maximum safety, this study examines the high-risk flood areas in an exceptional storm event scenario, and the SSP5-8.5 low confidence scenario with sea level projections of 0.928 m and 2.428 m in 2060 and 2100, respectively. The effects of future flood hazards, caused by climate change, on future urban development were analyzed by overlaying the three urban growth scenarios (business as usual, environmental protection, strategic urban planning) for the years 2060 and 2100 with high-risk flood areas and projected sea level rise.

3. Results and Discussion

3.1. Accuracy of LULC Map Classification

The LULC classification was carried out using a random forest model with median Landsat 5 and 8 images for the years 2006, 2019, and 2022, as detailed in Section 2. Based on past research, the median temporal aggregation approach used in this study greatly reduced the volume of data, resulting in quicker and easier analysis and improved accuracy, comparable to that of time series data [44].

Figure 3a–c shows the LULC maps of the study area created for the three years, and Table 4 summarizes the accuracy of the findings for each of the sample years. For the 2006, 2019, and 2022 LULC maps, the random forest classification performed well, with overall accuracies of 93.26%, 95.11%, and 94.04%, and kappa values of 0.91, 0.93, and 0.92, respectively. These assessment metrics were calculated using the error matrix for each LULC map (Table 5), indicating a high overall accuracy for the random forest classification despite some minor classification errors between urban areas and certain agricultural and other lands due to similar spectral signatures. Classification mistakes caused by spectral confusion across LULC classes with comparable spectral responses are acknowledged drawbacks in LULC classification in the literature [66,67]. Nevertheless, the modeling skills obtained exceed the recommended threshold of 80%, suggesting that the random forest classification is suitable for the requirements of the study.

Table 4. Accuracy assessment of LULC map classification.

Accuracy	LULC 2006	LULC 2019	LULC 2022
Overall accuracy (%)	93.26	95.11	94.04
Kappa coefficient (K)	0.91	0.93	0.92

Table 5. Error matrices for the classified LULC maps.

Year	Classified Data	Reference Data				
		Water	Forest	Other Land	Agriculture	Urban
2022	Water	212	6	6	4	0
	Forest	0	204	0	5	0
	Other land	3	0	207	2	8
	Agriculture	1	1	0	400	13
	Urban	0	0	6	22	193
2019	Water	229	4	2	0	0
	Forest	3	224	0	3	0
	Other land	1	0	202	1	3
	Agriculture	1	3	0	391	26
	Urban	0	1	4	11	180
2006	Water	203	1	0	5	0
	Forest	0	203	0	2	0
	Other land	0	0	217	3	7
	Agriculture	1	2	0	365	26
	Urban	0	0	9	29	190

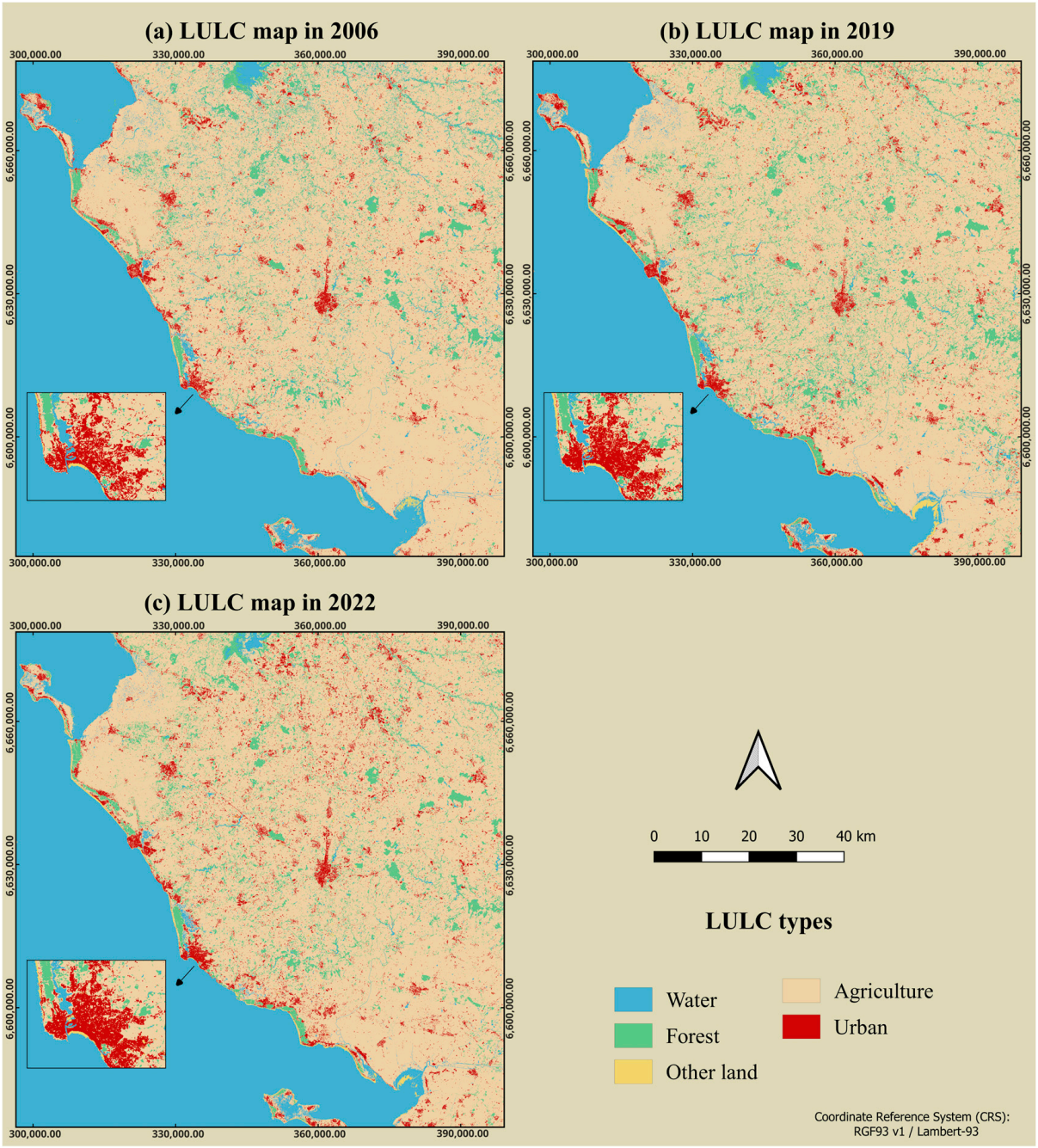

Figure 3. LULC classification: (**a**) LULC in 2006; (**b**) LULC in 2019; (**c**) LULC in 2022.

3.2. Model Validation and Prediction of Future Urban Growth

The transition observed between 2006 and 2019 was used to calibrate the MLP–Markov model and simulate future urban expansion. During this period, the study area underwent 32.24 km^2 of urban expansion, with urban areas increasing from 316.79 km^2 in 2006 to 349.03 km^2 in 2019. The model showed 81.11% accuracy for the calibration period. This accuracy is acceptable according to previous studies [4,27,30]. The reference map and the simulated 2022 LULC maps were compared to validate the calibrated model; Table 6 displays the validation metrics for the combined MLP–Markov model. All variations of the kappa index for all three scenarios, including Kno, Kappa Kstandard, and Klocation, were greater than 80%, demonstrating good agreement between the reference and simulated maps. The quantity disagreement remained consistent for all the scenarios at 2.16%, while

the allocation disagreement was 6.4%, indicating that the disagreements were mainly due to location error rather than quantity error. The results achieved by Al Rifat and Liu were comparable to our results, suggesting that the disagreements between the observed and simulated maps are primarily due to location error rather than quantity error [4]. Finally, the overall agreement achieved was 91%, and the AUC varied between 61.77% and 63.80% in all three scenarios. Although the model predicted the same level of urbanization in all scenarios, the location of the urban areas predicted varied according to the constraints applied in each scenario. The overall accuracy of the MLP–Markov prediction can be considered good and acceptable across all three scenarios.

Table 6. Prediction accuracy of the combined MLP–Markov model.

Assessment Metrics	Urban Growth Scenarios		
	Business as Usual	Environmental Protection	Strategic Urban Planning
Kno	89.71	89.72	89.72
Kappa Kstandard	85.35	85.36	85.37
Klocation	88.63	88.64	88.65
Quantity disagreement	2.16	2.16	2.16
Allocation disagreement	6.41	6.41	6.40
Overall agreement	91.43	91.43	91.44
AUC	61.77	62.80	63.78

After testing the predictability of the model, it was used to simulate future urban expansion scenarios for 2060 and 2100, as shown in Figures 4 and 5, respectively. According to the results achieved, urban areas will account for 514.45 km^2 of the study area by 2060, and 679.87 km^2 by 2100, with a total urban expansion of 330.84 km^2 between 2019 and 2100. Although urban expansion levels were constant across the three scenarios, the spatial distribution of new urban areas within the study area differed depending on the limitations imposed in each scenario (Figures 4 and 5), with the predicted urban development across all scenarios mostly taking place in coastal zones. The following sites were selected to showcase the results of urban growth modeling more effectively, and they include Noirmoutier Island, Notre-Dame-de-Monts, Les Sables-d'Olonne, Ré Island, and the Sèvre Niortaise River, which have different landscapes with urban districts surrounded by natural or agriculture land.

As shown in Figures 4 and 5, the majority of future urban expansion under the business-as-usual scenario is predicted to occur in coastal areas, continuing from the periphery of the existing urban areas and extending along the road networks. This scenario demonstrates a substantial expansion of urban development into formerly forests or agricultural regions. All insets indicate larger red regions, indicating greater urban expansion.

The environmental-protection scenario indicates less urban growth than the business-as-usual scenario, with more forest and agricultural areas being preserved. Noirmoutier Island retains most of its natural state with limited urbanization, while Notre-Dame-de-Monts achieves a compromise between maintaining natural regions and permitting modest urban expansion. Les Sables-d'Olonne demonstrates managed urban growth that helps protect more natural areas and Ré Island demonstrates strategies that successfully control urban growth to conserve the island's natural ecosystem.

Finally, a more strategically planned urban growth is shown in the strategic-urban-planning scenario. While still expanding, the urban regions seem to be more controlled. Under this scenario, the pattern of future urban growth is consistent with the environmental-protection scenario, particularly at Notre-Dame-de-Monts and Les Sables-d'Olonne. Conversely, the Natural Risk Prevention Plan's development restrictions have led to decreased urbanization on Ré Island, Noirmoutier Island, and the Sèvre Niortaise River.

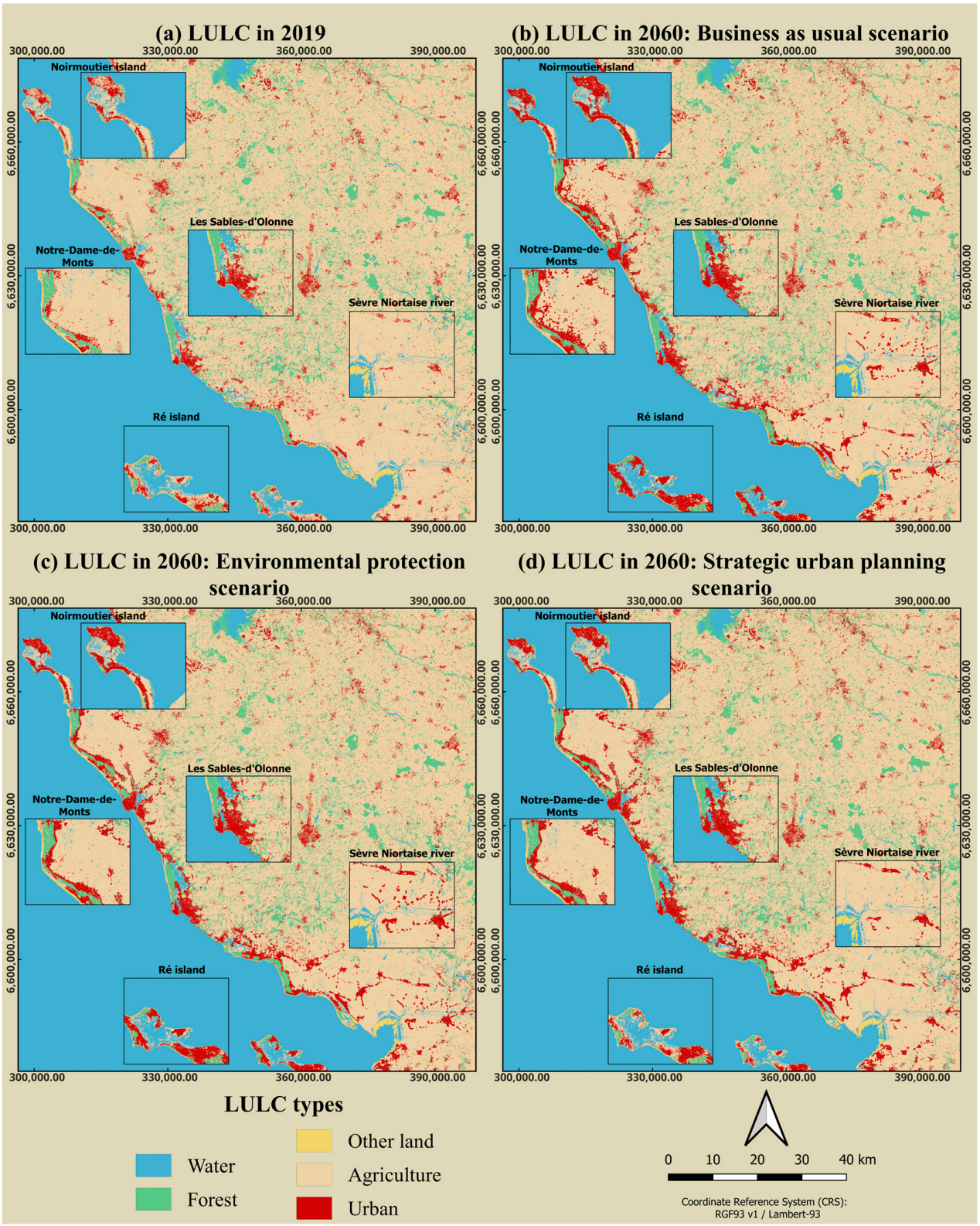

Figure 4. Prediction of urban growth scenarios in 2060: (**a**) LULC in 2019; (**b**) LULC in 2060 under the business-as-usual scenario; (**c**) LULC in 2060 under the environmental protection scenario; (**d**) LULC in 2060 under the strategic urban planning scenario.

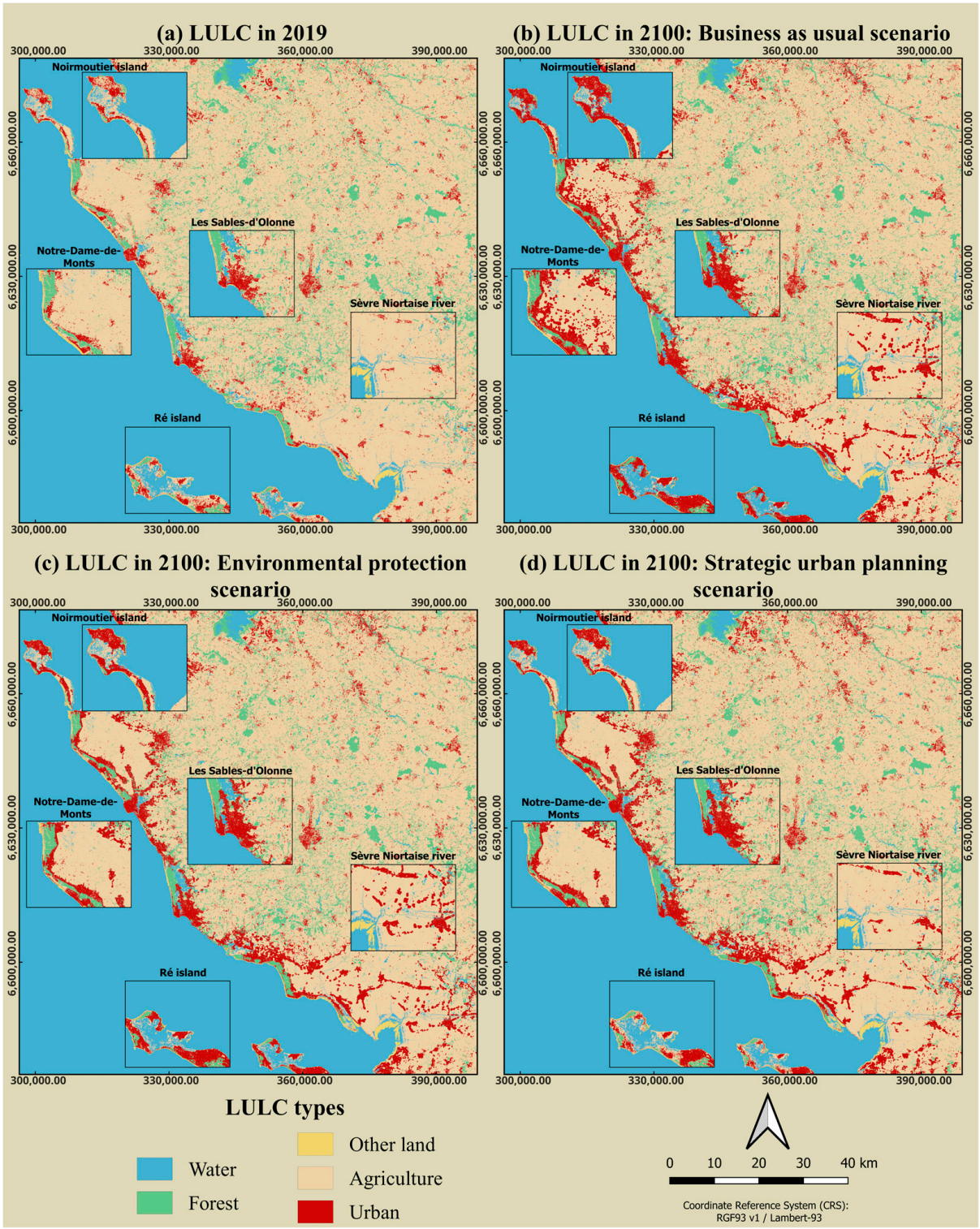

Figure 5. Prediction of urban growth scenarios in 2100: (**a**) LULC in 2019; (**b**) LULC in 2100 under the business-as-usual scenario; (**c**) LULC in 2100 under the environmental protection scenario; (**d**) LULC in 2100 under the strategic urban planning scenario.

3.3. Evaluation of Urban Exposure to Flooding

Exposure to urban flooding was analyzed by overlaying the predicted urban expansion scenarios with high-risk flood zones and projected sea level rise. The high-risk flood zones, i.e., areas susceptible to flooding due to extreme winter storms, covered an area of

623.279 km^2, and the sea level rise scenario used in this study extended the affected regions to 638.892 km^2 by 2060, and to 1392.87 km^2 by 2100. In 2019, 32.10 km^2, i.e., 9.19% of the existing urban areas, were already vulnerable to coastal flooding caused by severe storms (Figure 6a). As demonstrated in Figure 6b–d, the urban area exposed will rise due to urban expansion and rising sea levels.

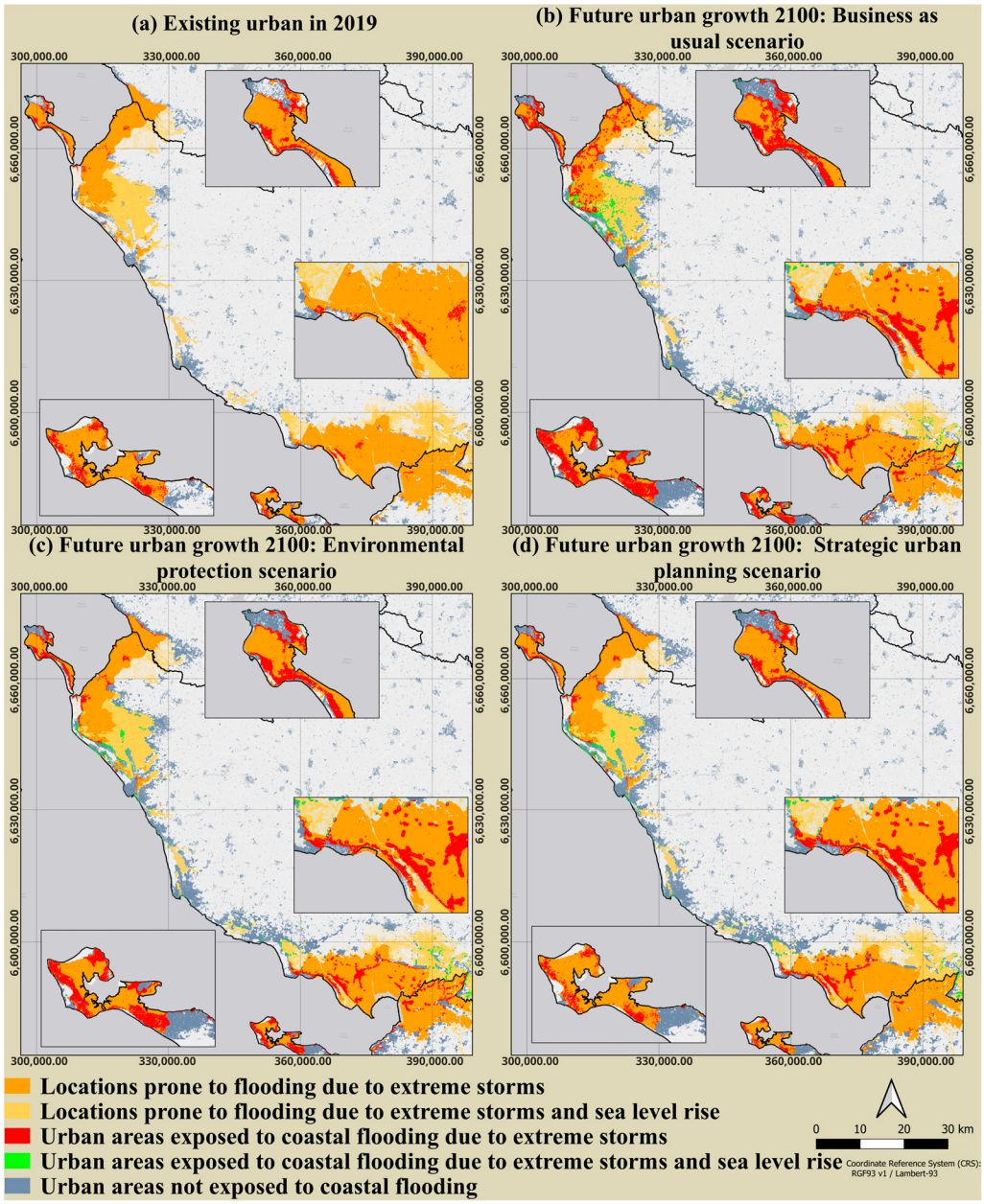

Figure 6. Future urban growth scenarios and exposure to flooding risk in 2100: (**a**) Urban exposure to flooding in 2019; (**b**) Urban exposure to flooding in 2100 under the business-as-usual scenario; (**c**) Urban exposure to flooding in 2100 under the environmental protection scenario; (**d**) Urban exposure to flooding in 2100 under the strategic urban planning scenario.

Under the business-as-usual scenario, 91.85 km^2 of urban areas will be at risk of flooding due to extreme storms by 2060, and with a rise of 0.928 m in sea level, the exposed areas would increase to 94.47 km^2. The situation was predicted to be worse in 2100, with an exposed area of 129.43 km^2, and more places would be vulnerable to floods with a 2.428 m rise in sea level by 2100, resulting in a total exposed area of 225.97 km^2 (Table 7).

Table 7. Urban flood exposure and sea level rise impact.

Year	Total Urban Area (km^2)	Urban Growth Scenario	Urban Areas Susceptible to Flooding Due to Extreme Storms (km^2)	Urban Areas Susceptible to Flooding Due to Extreme Storms and Sea Level Rise (km^2)
2060	514.45	Business as usual	91.8592	94.4719
		Environmental protection	78.139	79.6219
		Strategic urban planning	58.3806	59.6068
2100	679.87	Business as usual	129.434	225.97
		Environmental protection	98.8963	165.263
		Strategic urban planning	68.4748	117.047

In the environmental-protection scenario, 78.13 km^2 and 98.89 km^2 of urban areas would be placed in high-risk flood zones by 2060 and 2100 respectively. Considering the increasing sea level rise scenario, the urban areas vulnerable to floods would grow to 79.621 km^2 and 165.26 km^2 by 2060 and 2100, respectively (Table 7). The amount of the urban area susceptible to flooding in this scenario was lower than in the business-as-usual scenario, indicating that the environmental-protection scenario represents an improved flood risk reduction in the future.

Finally, the urban areas vulnerable to floods under the strategic-urban-planning scenario are predicted to reach 58.38 km^2 in 2060 and 68.47 km^2 in 2100. These areas will extend to 59.60 km^2 and 117.04 km^2 by 2060 and 2100 respectively, taking sea level rise into consideration (Table 7). Although the strategic-urban-planning scenario exposes considerable sections of the urban area to flooding, it is the most effective of the three urban expansion scenarios for mitigating potential future flood risk.

The evaluation of the Vendée coast's possible vulnerability to flooding under several future expansion scenarios has important implications for urban planning and flood risk management. The business-as-usual scenario, which results in the biggest rise in flood-prone urban areas, emphasizes the vulnerability of unplanned or poorly managed urban growth to the effects of climate change. In contrast, the environmental-protection and strategic-urban-planning scenarios show much lower risks, demonstrating the efficacy of including regulations and restrictions in urban growth strategies.

The practical relevance of these results resides in their potential to support local authorities in developing better-informed and rigorous planning policies. The lower flood risk exposure in the environmental-protection scenario, for example, implies that policies promoting nature preservation and conservation might greatly decrease future flood risks. Similarly, the strategic-urban-planning scenario, which projects the least amount of future flood risk, provides a basic model for how urban areas might be planned to support development while reducing susceptibility.

For all three scenarios, the impact of sea level rise in 2060 is limited, with an increase of 1 to 3 km^2 in the exposed area. However, urban flood exposure will increase dramatically by 2100 due to the effects of the future rise in sea level. Even the best growth-case scenario in strategic urban planning, which is based on the local urban plan and considers the natural hazards threatening the study area, is questionable in terms of sustainability, as extensive urban areas will still be vulnerable to floods, highlighting the need for more urbanization regulations in the study area.

The guiding inspirations gained from this research are:

Policy implementation: The results highlight the crucial need for stricter urbanization restrictions and more effective planning measures. Incorporating the consequences of the extreme sea level rise scenario into planning efforts is critical for successfully limiting flood hazards in the studied region.

Proactive planning: The findings underscore the need to implement climate adaptation strategies proactively to manage anticipated rises in sea level and storm severity, as well as to address urban areas' increased susceptibility to flooding.

Sustainable urban development: The necessity for long-term urban development policies that not only handle population shifts but also move the upcoming urban expansion away from coastal locations that are susceptible to flooding.

In conclusion, this study offers a detailed and evidence-based roadmap toward sustainable urban development and flood risk mitigation. It underlines the need to incorporate extensive flood risk assessments into the planning process in order to direct future urban expansion away from susceptible locations. The findings emphasize the crucial need of taking proactive actions to limit urban areas' rising susceptibility to flooding, which is consistent with the major focus of our research on sustainable urban planning and flood risk reduction in coastal zones.

Despite the progress presented in our study, more research is needed to increase the accuracy of the prediction of urban growth scenarios, which could also extend to other urban growth models in order to identify the best predictive model for the study area. This study was limited to the use of six variables representing the driving forces of urban expansion. Therefore, future research should incorporate more driving variables, which would increase the prediction accuracy of the urban growth model.

4. Conclusions

This study concerns the use of an urban growth modeling technique to simulate future urban growth scenarios and assess the implications of potential flood risk on future urban expansion along the Vendée coastal region in western France. The main objective of the study is to contribute to sustainable urban planning and flood risk mitigation by identifying and assessing the potential impacts of extreme storm events and rising sea levels on future urban flood exposure. The contributions made by the research are the incorporation of urban growth modeling based on different growth scenarios with both climate change and flood risk and the application of the MLP–Markov model, which is rarely used for estimating future exposure of urban areas to flooding. Additionally, the research examines not only the impacts of sea level rise but also those of extreme storm events.

A LULC classification was first carried out in GEE using a random forest model with Landsat 5 and 8 images to generate LULC maps of the study area for 2006, 2019, and 2022. The classification findings demonstrated high accuracy and the LULC maps that were created enable the examination of historical urban expansion, which is in keeping with the research requirements.

An MLP–Markov model was then used to forecast three future urban expansion scenarios: business as usual, environmental protection, and strategic urban planning. The simulation predicted potential urban growth for the year 2022 based on observed changes between 2006 and 2019, and the model was validated by comparing the simulated maps to the 2022 LULC map. The evaluation of the model indicated good agreement between the reference map and the simulated maps, as evidenced by all variants of the kappa index (Kno, Kappa Kstandard, and Klocation) surpassing 80%, overall agreement exceeding 90%, and AUC values exceeding 60% for all three scenarios. The model provided satisfactory results with only minor disagreements, mostly due to location errors, with quantity disagreement accounting for 2.16%, and allocation disagreement around 6.4% across all scenarios. The assessment of the MLP–Markov model demonstrated its effectiveness in simulating reasonable outputs for future urban expansion. After evaluating the prediction capacity of the model, it was utilized to simulate future urban growth scenarios for 2060 and 2100. The findings revealed that different urban growth scenarios forecast diverse development patterns. While all scenarios predicted similar levels of urban expansion, the constraints imposed in the different scenarios affected the geographical distribution of the new urban areas.

Finally, to identify future flood-risk zones in 2060 and 2100, the predicted urban expansion scenarios were overlapped with high-risk flood areas and estimated sea level rise. Given the uncertainties surrounding future climate change, and to better prepare

for the worst-case scenario, this study looked at high-risk flood areas associated with exceptional storm events and extreme sea level rise scenarios.

The research results show that regulations and urbanization management can help limit exposure to urban floods in the future. The strategic-urban-planning scenario, which has the greatest limitations and regulations, produced the fewest urban areas vulnerable to floods, followed by the environmental-protection scenario, and lastly the business-as-usual scenario, which does not include development policies. The strategic-urban-planning scenario, which incorporates protected and environmentally-sensitive regions as well as development regulations from the Natural Risk Prevention Plan, is the most effective urban growth scenario for flood risk reduction. However, the incorporation of sea level rise projections reveals that susceptible zones are anticipated to increase significantly. Despite the limitations and controls being imposed in the strategic urban planning scenario, the study area is anticipated to experience a considerable increase in urban flood exposure by 2100 due to further rises in sea level.

These results demonstrate the crucial importance of including flood risk assessment in urban expansion modeling efforts and underline the need of taking proactive actions to address urban areas' increased susceptibility to flooding. While the short-term impact of sea level rise is limited, the long-term estimates highlight the urgency of imposing stronger urbanization constraints and more efficient planning strategies. Incorporating the impacts of the extreme sea level rise scenario into future planning efforts is crucial for effectively limiting flood risks in the study area and moving upcoming urban expansion away from coastal sites that are prone to flooding.

The urban growth modeling technique used in this study predicts future development sites as well as the number of urban areas vulnerable to future flooding, which allows us to examine the consequences of various development paths on future flood risk. It can therefore assist policymakers and urban planners to better prepare for the impacts of climate change by laying the groundwork for the development of mitigation and adaptation measures.

Author Contributions: Methodology, A.F., M.M. (Mohamed Maanan), M.M. (Mehdi Maanan) and H.R.; Validation, A.F., M.M. (Mohamed Maanan), M.M. (Mehdi Maanan) and H.R.; Investigation, A.F., M.M. (Mohamed Maanan) and H.R.; Data curation, A.F.; Writing—original draft, A.F., M.M. (Mohamed Maanan), M.M. (Mehdi Maanan) and H.R.; Supervision, M.M. (Mohamed Maanan) and H.R.; Project administration, M.M. (Mohamed Maanan). All authors have read and agreed to the published version of the manuscript.

Funding: This research received no external funding.

Institutional Review Board Statement: Not applicable.

Informed Consent Statement: Not applicable.

Data Availability Statement: All data utilized in this study are publicly accessible, with their respective sources provided in the 'Data Used' section within the main text.

Acknowledgments: The authors would like to express their gratitude to the UMR 6554 CNRS LETG-Nantes laboratory for their support during the research stay, conducted as part of the international co-supervision of Ayyoub Frifra's thesis. Additionally, this work received support from the CNRST Morocco (Centre National pour la Recherche Scientifique et Technique), under the research excellence scholarship program. This research is also an integral part of the CNRS MITI MOGEC research project led by MAANAN.

Conflicts of Interest: The authors declare no conflict of interest.

References

1. Carter, J.G. Urban Climate Change Adaptation: Exploring the Implications of Future Land Cover Scenarios. *Cities* **2018**, *77*, 73–80. [CrossRef]
2. Hinkel, J.; Lincke, D.; Vafeidis, A.T.; Perrette, M.; Nicholls, R.J.; Tol, R.S.J.; Marzeion, B.; Fettweis, X.; Ionescu, C.; Levermann, A. Coastal Flood Damage and Adaptation Costs under 21st Century Sea-Level Rise. *Proc. Natl. Acad. Sci. USA* **2014**, *111*, 3292–3297. [CrossRef]
3. Seto, K.C.; Güneralp, B.; Hutyra, L.R. Global Forecasts of Urban Expansion to 2030 and Direct Impacts on Biodiversity and Carbon Pools. *Proc. Natl. Acad. Sci. USA* **2012**, *109*, 16083–16088. [CrossRef]
4. Rifat, S.A.A.; Liu, W. Predicting Future Urban Growth Scenarios and Potential Urban Flood Exposure Using Artificial Neural Network-Markov Chain Model in Miami Metropolitan Area. *Land Use Policy* **2022**, *114*, 105994. [CrossRef]
5. Neumann, B.; Vafeidis, A.T.; Zimmermann, J.; Nicholls, R.J. Future Coastal Population Growth and Exposure to Sea-Level Rise and Coastal Flooding—A Global Assessment. *PLoS ONE* **2015**, *10*, e0118571. [CrossRef]
6. Brown, S.; Nicholls, R.J.; Woodroffe, C.D.; Hanson, S.; Hinkel, J.; Kebede, A.S.; Neumann, B.; Vafeidis, A.T. Sea-Level Rise Impacts and Responses: A Global Perspective. *Coast. Res. Libr.* **2013**, *1000*, 117–149. [CrossRef]
7. Kron, W. Coasts: The High-Risk Areas of the World. *Nat. Hazards* **2013**, *66*, 1363–1382. [CrossRef]
8. Tzepkenlis, A.; Grammalidis, N.; Kontopoulos, C.; Charalampopoulou, V.; Kitsiou, D.; Pataki, Z.; Patera, A.; Nitis, T. An Integrated Monitoring System for Coastal and Riparian Areas Based on Remote Sensing and Machine Learning. *J. Mar. Sci. Eng.* **2022**, *10*, 1322. [CrossRef]
9. Breilh, J.F.; Bertin, X.; Chaumillon, É.; Giloy, N.; Sauzeau, T. How Frequent Is Storm-Induced Flooding in the Central Part of the Bay of Biscay? *Glob. Planet. Change* **2014**, *122*, 161–175. [CrossRef]
10. Nicholls, R.J. Planning for the Impacts of Sea Level Rise. *Oceanography* **2011**, *24*, 144–157. [CrossRef]
11. Nicholls, R.J. Coastal Flooding and Wetland Loss in the 21st Century: Changes under the SRES Climate and Socio-Economic Scenarios. *Glob. Environ. Change* **2004**, *14*, 69–86. [CrossRef]
12. Ranasinghe, R. Assessing Climate Change Impacts on Open Sandy Coasts: A Review. *Earth Sci. Rev.* **2016**, *160*, 320–332. [CrossRef]
13. Masson-Delmotte, V.; Zhai, P.; Pirani, S.; Connors, C.; Péan, S.; Berger, N.; Caud, Y.; Chen, L.; Goldfarb, M.; Scheel Monteiro, P.M. IPCC, 2021: Summary for Policymakers. In *Climate Change 2021—The Physical Science Basis: Working Group I Contribution to the Sixth Assessment Report of the Intergovernmental Panel on Climate Change*; Cambridge University Press: Cambridge, UK, 2021. [CrossRef]
14. Chen, Y. An Extended Patch-Based Cellular Automaton to Simulate Horizontal and Vertical Urban Growth under the Shared Socioeconomic Pathways. *Comput. Environ. Urban Syst.* **2022**, *91*, 101727. [CrossRef]
15. Clarke, K.C.; Hoppen, S.; Gaydos, L. A Self-Modifying Cellular Automaton Model of Historical Urbanization in the San Francisco Bay Area. *Environ. Plan. B Plan. Des.* **1997**, *24*, 247–261. [CrossRef]
16. Vaz, E.d.N.; Nijkamp, P.; Painho, M.; Caetano, M. A Multi-Scenario Forecast of Urban Change: A Study on Urban Growth in the Algarve. *Landsc. Urban Plan.* **2012**, *104*, 201–211. [CrossRef]
17. Kamusoko, C.; Gamba, J. Simulating Urban Growth Using a Random Forest-Cellular Automata (RF-CA) Model. *ISPRS Int. J. Geo-Inf.* **2015**, *4*, 447–470. [CrossRef]
18. Chaudhuri, G.; Clarke, K.C. Modeling an Indian Megalopolis– A Case Study on Adapting SLEUTH Urban Growth Model. *Comput. Environ. Urban Syst.* **2019**, *77*, 101358. [CrossRef]
19. Silva, E.A.; Clarke, K.C. Calibration of the SLEUTH Urban Growth Model for Lisbon and Porto, Portugal. *Comput. Environ. Urban Syst.* **2002**, *26*, 525–552. [CrossRef]
20. Shafizadeh-Moghadam, H. Improving Spatial Accuracy of Urban Growth Simulation Models Using Ensemble Forecasting Approaches. *Comput. Environ. Urban Syst.* **2019**, *76*, 91–100. [CrossRef]
21. Yang, X.; Chen, R.; Zheng, X.Q. Simulating Land Use Change by Integrating ANN-CA Model and Landscape Pattern Indices. *Geomat. Nat. Hazards Risk* **2015**, *7*, 918–932. [CrossRef]
22. Guan, D.J.; Li, H.F.; Inohae, T.; Su, W.; Nagaie, T.; Hokao, K. Modeling Urban Land Use Change by the Integration of Cellular Automaton and Markov Model. *Ecol. Modell.* **2011**, *222*, 3761–3772. [CrossRef]
23. Shafizadeh Moghadam, H.; Helbich, M. Spatiotemporal Urbanization Processes in the Megacity of Mumbai, India: A Markov Chains-Cellular Automata Urban Growth Model. *Appl. Geogr.* **2013**, *40*, 140–149. [CrossRef]
24. Tang, J.; Wang, L.; Yao, Z. Spatio-Temporal Urban Landscape Change Analysis Using the Markov Chain Model and a Modified Genetic Algorithm. *Int. J. Remote Sens.* **2007**, *28*, 3255–3271. [CrossRef]
25. Thapa, R.B.; Murayama, Y. Scenario Based Urban Growth Allocation in Kathmandu Valley, Nepal. *Landsc. Urban Plan.* **2012**, *105*, 140–148. [CrossRef]
26. Iizuka, K.; Johnson, B.A.; Onishi, A.; Magcale-Macandog, D.B.; Endo, I.; Bragais, M. Modeling Future Urban Sprawl and Landscape Change in the Laguna de Bay Area, Philippines. *Land* **2017**, *6*, 26. [CrossRef]
27. Simwanda, M.; Murayama, Y.; Phiri, D.; Nyirenda, V.R.; Ranagalage, M. Simulating Scenarios of Future Intra-Urban Land-Use Expansion Based on the Neural Network–Markov Model: A Case Study of Lusaka, Zambia. *Remote Sens.* **2021**, *13*, 942. [CrossRef]
28. Lu, Y.; Wang, X.; Xie, Y.; Li, K.; Xu, Y. Integrating Future Land Use Scenarios to Evaluate the Spatio-Temporal Dynamics of Landscape Ecological Security. *Sustainability* **2016**, *8*, 1242. [CrossRef]

29. Shi, Y.; Wu, J.; Shi, S. Study of the Simulated Expansion Boundary of Construction Land in Shanghai Based on a SLEUTH Model. *Sustainability* **2017**, *9*, 876. [CrossRef]
30. Ranagalage, M.; Wang, R.; Gunarathna, M.H.J.P.; Dissanayake, D.M.S.L.B.; Murayama, Y.; Simwanda, M. Spatial Forecasting of the Landscape in Rapidly Urbanizing Hill Stations of South Asia: A Case Study of Nuwara Eliya, Sri Lanka (1996–2037). *Remote Sens.* **2019**, *11*, 1743. [CrossRef]
31. Nath, B.; Wang, Z.; Ge, Y.; Islam, K.; Singh, R.P.; Niu, Z. Land Use and Land Cover Change Modeling and Future Potential Landscape Risk Assessment Using Markov-CA Model and Analytical Hierarchy Process. *ISPRS Int. J. Geo-Inf.* **2020**, *9*, 134. [CrossRef]
32. Hinestroza-Mena, K.M.; Toro, V.G.; Londoño-Colorado, G.S.; Chávez, V.; García-Blanco, J.K.; Silva, R. Fine Spatial Scale, Frequent Morphological Monitoring of Urbanised Beaches to Improve Coastal Management. *J. Mar. Sci. Eng.* **2021**, *9*, 550. [CrossRef]
33. Tsagkis, P.; Bakogiannis, E.; Nikitas, A. Analysing Urban Growth Using Machine Learning and Open Data: An Artificial Neural Network Modelled Case Study of Five Greek Cities. *Sustain. Cities Soc.* **2023**, *89*, 104337. [CrossRef]
34. Abouhalima, M.; das Neves, L.; Taveira-Pinto, F.; Rosa-Santos, P. Machine Learning in Coastal Engineering: Applications, Challenges, and Perspectives. *J. Mar. Sci. Eng.* **2024**, *12*, 638. [CrossRef]
35. Huong, H.T.L.; Pathirana, A. Urbanization and Climate Change Impacts on Future Urban Flooding in Can Tho City, Vietnam. *Hydrol. Earth Syst. Sci.* **2013**, *17*, 379–394. [CrossRef]
36. Lu, Q.; Joyce, J.; Imen, S.; Chang, N. Bin Linking Socioeconomic Development, Sea Level Rise, and Climate Change Impacts on Urban Growth in New York City with a Fuzzy Cellular Automata-Based Markov Chain Model. *Environ. Plan. B Urban Anal. City Sci.* **2019**, *46*, 551–572. [CrossRef]
37. Song, J.; Fu, X.; Gu, Y.; Deng, Y.; Peng, Z.R. An Examination of Land Use Impacts of Flooding Induced by Sea Level Rise. *Nat. Hazards Earth Syst. Sci.* **2017**, *17*, 315–334. [CrossRef]
38. Audère, M.; Robin, M. Assessment of the Vulnerability of Sandy Coasts to Erosion (Short and Medium Term) for Coastal Risk Mapping (Vendée, W France). *Ocean Coast. Manag.* **2021**, *201*, 105452. [CrossRef]
39. Bertin, X.; Li, K.; Roland, A.; Zhang, Y.J.; Breilh, J.F.; Chaumillon, E. A Modeling-Based Analysis of the Flooding Associated with Xynthia, Central Bay of Biscay. *Coast. Eng.* **2014**, *94*, 80–89. [CrossRef]
40. Bertin, X.; Bruneau, N.; Breilh, J.F.; Fortunato, A.B.; Karpytchev, M. Importance of Wave Age and Resonance in Storm Surges: The Case Xynthia, Bay of Biscay. *Ocean. Model.* **2012**, *42*, 16–30. [CrossRef]
41. Kolen, B.; Slomp, R.; Jonkman, S.N. The Impacts of Storm Xynthia February 27–28, 2010 in France: Lessons for Flood Risk Management. *J. Flood Risk Manag.* **2013**, *6*, 261–278. [CrossRef]
42. Kron, W.; Löw, P.; Kundzewicz, Z.W. Changes in Risk of Extreme Weather Events in Europe. *Environ. Sci. Policy* **2019**, *100*, 74–83. [CrossRef]
43. Foga, S.; Scaramuzza, P.L.; Guo, S.; Zhu, Z.; Dilley, R.D.; Beckmann, T.; Schmidt, G.L.; Dwyer, J.L.; Joseph Hughes, M.; Laue, B. Cloud Detection Algorithm Comparison and Validation for Operational Landsat Data Products. *Remote Sens. Environ.* **2017**, *194*, 379–390. [CrossRef]
44. Noi Phan, T.; Kuch, V.; Lehnert, L.W. Land Cover Classification Using Google Earth Engine and Random Forest Classifier-the Role of Image Composition. *Remote Sens.* **2020**, *12*, 2411. [CrossRef]
45. Jin, Y.; Liu, X.; Chen, Y.; Liang, X. Land-Cover Mapping Using Random Forest Classification and Incorporating NDVI Time-Series and Texture: A Case Study of Central Shandong. *Int. J. Remote Sens.* **2018**, *39*, 8703–8723. [CrossRef]
46. Li, X.; Chen, W.; Cheng, X.; Wang, L. A Comparison of Machine Learning Algorithms for Mapping of Complex Surface-Mined and Agricultural Landscapes Using ZiYuan-3 Stereo Satellite Imagery. *Remote Sens.* **2016**, *8*, 514. [CrossRef]
47. Millard, K.; Richardson, M. On the Importance of Training Data Sample Selection in Random Forest Image Classification: A Case Study in Peatland Ecosystem Mapping. *Remote Sens.* **2015**, *7*, 8489–8515. [CrossRef]
48. Nasiri, V.; Deljouei, A.; Moradi, F.; Sadeghi, S.M.M.; Borz, S.A. Land Use and Land Cover Mapping Using Sentinel-2, Landsat-8 Satellite Images, and Google Earth Engine: A Comparison of Two Composition Methods. *Remote Sens.* **2022**, *14*, 1977. [CrossRef]
49. Sheykhmousa, M.; Mahdianpari, M.; Ghanbari, H.; Mohammadimanesh, F.; Ghamisi, P.; Homayouni, S. Support Vector Machine Versus Random Forest for Remote Sensing Image Classification: A Meta-Analysis and Systematic Review. *IEEE J. Sel. Top. Appl. Earth Obs. Remote Sens.* **2020**, *13*, 6308–6325. [CrossRef]
50. Maxwell, A.E.; Warner, T.A.; Fang, F. Implementation of Machine-Learning Classification in Remote Sensing: An Applied Review. *Int. J. Remote Sens.* **2018**, *39*, 2784–2817. [CrossRef]
51. Pelletier, C.; Valero, S.; Inglada, J.; Champion, N.; Dedieu, G. Assessing the Robustness of Random Forests to Map Land Cover with High Resolution Satellite Image Time Series over Large Areas. *Remote Sens. Environ.* **2016**, *187*, 156–168. [CrossRef]
52. Tamiminia, H.; Salehi, B.; Mahdianpari, M.; Quackenbush, L.; Adeli, S.; Brisco, B. Google Earth Engine for Geo-Big Data Applications: A Meta-Analysis and Systematic Review. *ISPRS J. Photogramm. Remote Sens.* **2020**, *164*, 152–170. [CrossRef]
53. Breiman, L. Random Forests. *Mach. Learn.* **2001**, *45*, 5–32. [CrossRef]
54. Breiman, L. Bagging Predictors. *Mach. Learn.* **1996**, *24*, 123–140. [CrossRef]
55. Abdullah, S.A.; Nakagoshi, N. Changes in Landscape Spatial Pattern in the Highly Developing State of Selangor, Peninsular Malaysia. *Landsc. Urban Plan.* **2006**, *77*, 263–275. [CrossRef]
56. Qiang, Y.; Lam, N.S.N. The Impact of Hurricane Katrina on Urban Growth in Louisiana: An Analysis Using Data Mining and Simulation Approaches. *Int. J. Geogr. Inf. Sci.* **2016**, *30*, 1832–1852. [CrossRef]

57. Zhang, D.; Liu, X.; Wu, X.; Yao, Y.; Wu, X.; Chen, Y. Multiple Intra-Urban Land Use Simulations and Driving Factors Analysis: A Case Study in Huicheng, China. *GIsci Remote Sens.* **2019**, *56*, 282–308. [CrossRef]
58. Abuelaish, B.; Olmedo, M.T.C. Scenario of Land Use and Land Cover Change in the Gaza Strip Using Remote Sensing and GIS Models. *Arab. J. Geosci.* **2016**, *9*, 274. [CrossRef]
59. Nadoushan, M.A.; Soffianian, A.; Alebrahim, A. Predicting Urban Expansion in Arak Metropolitan Area Using Two Land Change Models. *World Appl. Sci. J.* **2012**, *18*, 1124–1132. [CrossRef]
60. Pontius, R.G. Quantification Error versus Location Error in Comparison of Categorical Maps. *Photogramm. Eng. Remote Sens.* **2000**, *66*, 1011–1016.
61. Islam, K.; Rahman, M.F.; Jashimuddin, M. Modeling Land Use Change Using Cellular Automata and Artificial Neural Network: The Case of Chunati Wildlife Sanctuary, Bangladesh. *Ecol. Indic.* **2018**, *88*, 439–453. [CrossRef]
62. Pontius, R.G.; Millones, M. Death to Kappa: Birth of Quantity Disagreement and Allocation Disagreement for Accuracy Assessment. *Int. J. Remote Sens.* **2011**, *32*, 4407–4429. [CrossRef]
63. Pontius, R.G.; Parmentier, B. Recommendations for Using the Relative Operating Characteristic (ROC). *Landsc. Ecol.* **2014**, *29*, 367–382. [CrossRef]
64. Pontius, R.G.; Schneider, L.C. Land-Cover Change Model Validation by an ROC Method for the Ipswich Watershed, Massachusetts, USA. *Agric. Ecosyst. Environ.* **2001**, *85*, 239–248. [CrossRef]
65. Masson-Delmotte, V.; Zhai, P.; Chen, Y.; Goldfarb, L.; Gomis, M.I.; Matthews, J.B.R.; Berger, S.; Huang, M.; Yelekçi, O.; Yu, R.; et al. *Working Group I Contribution to the Sixth Assessment Report of the Intergovernmental Panel on Climate Change*; Cambridge University Press: Cambridge, UK, 2021. [CrossRef]
66. Osgouei, P.E.; Kaya, S.; Sertel, E.; Alganci, U. Separating Built-up Areas from Bare Land in Mediterranean Cities Using Sentinel-2A Imagery. *Remote Sens.* **2019**, *11*, 345. [CrossRef]
67. Zhao, Y.; Zhu, Z. ASI: An Artificial Surface Index for Landsat 8 Imagery. *Int. J. Appl. Earth Obs. Geoinf.* **2022**, *107*, 102703. [CrossRef]